Boosting mRNA cancer vaccine efficacy via targeting *Irg1* on macrophages in lymph nodes

Wenwen Wei*[1,2,3], Xiao Yang*[1,2,3], Yeshan Chen*[1,2,3], Mengjie Che*[1,2,3], Ying Ye[1,2,3], Yue Deng[1,2,3], Mengyao Su[1,2,3], Yajie Sun[1,2,3], Jingshu Meng[1,2,3], Yan Hu[1,2,3], Jiacheng Wang[1,2,3], Yijun Wang[1,2,3], Zishan Feng[1,2,3], Zhiyuan Zhou[1,2,3], Yan Li[1,2,3], Qian Li[1,2,3], Zhanjie Zhang[1,2,3],Bian Wu[1,2,3], Haibo Zhang[4], You Qin[1,2,3], Lu Wen[1,2,3], Chao Wan[#1,2,3], Kunyu Yang[#1,2,3]

1. Cancer Center, Union Hospital, Tongji Medical College, Huazhong University of Science and Technology, Wuhan 430022, China

2. Institute of Radiation Oncology, Union Hospital, Tongji Medical College, Huazhong University of Science and Technology, Wuhan 430022, China

3. Hubei Key Laboratory of Precision Radiation Oncology, Wuhan 430022, China

4. Cancer Center, Department of Radiation Oncology, Zhejiang Provincial People's Hospital (Affiliated People's Hospital), Hangzhou Medical College, Hangzhou, Zhejiang 310000, China

* These authors have contributed equally to this article.

[#] Corresponding authors: E-mail: Kunyu Yang, yangkunyu@hust.edu.cn; Chao Wan, wanc@hust.edu.cn

Graphical Abstracts

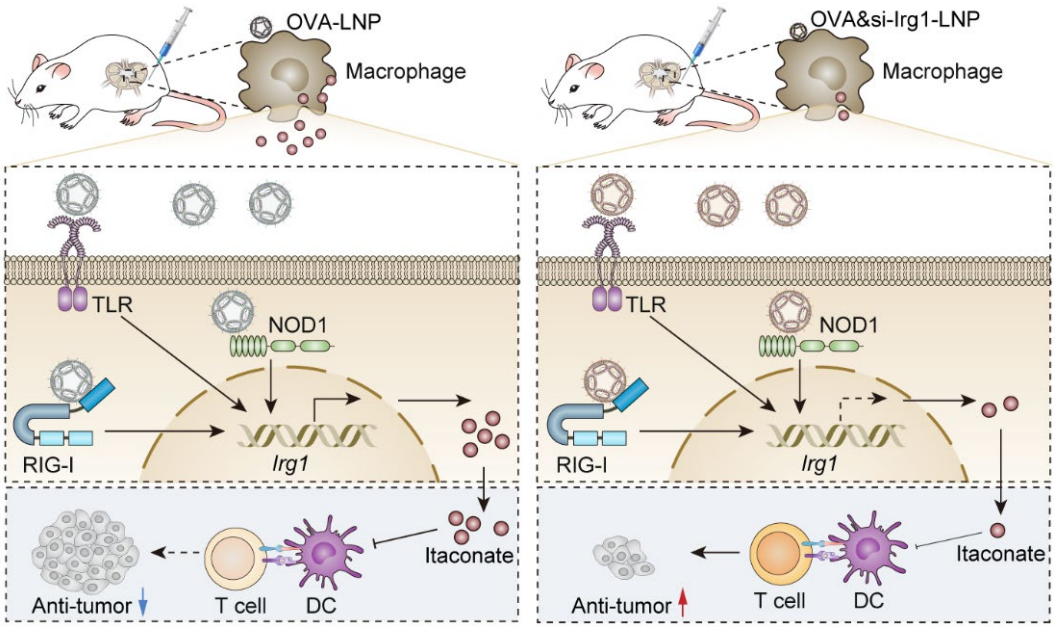

Abstract

Rationale: mRNA cancer vaccines show great promise for tumor therapy, but the therapeutic efficacy is limited. Metabolites play critical roles in immunomodulation. However, their role in mRNA cancer vaccines remains poorly understood.

Methods: Metabolome analysis and single-cell RNA sequence were performed to explore the most important metabolite and its source cell. B16-F10-OVA-bearing wide-type and *Irg1*-depleted C57BL/6 mice were treated with OVA-LNP, OVA&si-Irg1-LNP, or anti-PD-1 antibody to evaluate therapeutic efficacy. Flow cytometry analysis was used to examine the immune cells within the lymph nodes, spleens, and the tumor immune environment.

Results: We found that macrophage-derived itaconate was increased markedly in activated ipsilateral lymph nodes after ovalbumin-encoding mRNA-lipid nanoparticle (OVA-LNP) injection, compared to homeostatic contralateral lymph nodes. Depleting the immune-responsive gene 1(*Irg1*), which encodes the itaconate-production enzyme

aconitate decarboxylase (ACOD1), in macrophages improved dendritic cell antigen presentation and enhances T cell function. Combining *Irg1* knockdown via small interfering RNA (siRNA) with OVA mRNA in LNPs augmented the therapeutic efficacy of mRNA cancer vaccines, both as monotherapy and in combination with an anti-programmed cell death-1 antibody.

Conclusions: Our findings reveal a link between itaconate and mRNA cancer vaccines, suggesting that targeting *Irg1 via* siRNA-LNP could be a promising strategy to improve the therapeutic efficacy of mRNA cancer vaccines.

Keywords: Itaconate, mRNA cancer vaccines, macrophages, DCs, anti-PD-1 antibody

Introduction

The first mRNA cancer vaccine, encoding carcinoembryonic antigen (CEA), was shown to induce an immune response to CEA-expressing tumor cells in mice in 1995[1]. Since then, various *in vitro* preclinical studies of mRNAs have been conducted, revealing the therapeutic potential of mRNA-based approaches. Compared to previous DNA-based therapeutics, mRNA-based therapies have the advantage of enabling efficient expression while reducing the risk of insertional mutagenesis and stable integration of DNA into the host genome [2]. However, challenges such as the inherent instability and high immunogenicity of naked mRNA, lack of suitable manufacturing methods, and inefficient delivery methods have hindered their advancement for a long time. The success of mRNA vaccines against COVID-19 has advanced mRNA technology and generated interest in mRNA-based tumor therapeutics [3, 4]. Chemical

57 modification, product purification, and sequence optimization have been attempted to
58 enhance mRNA stability, prolong translation, and reduce immunogenicity [5-7]. In
59 addition, mRNA-packaging nanotechnologies, such as encapsulating mRNA into
60 nanoparticles, can protect mRNA from RNase-mediated degradation in cellular fluids
61 and facilitate efficient delivery into cells and organs for subsequent translation. For
62 instance, the current research focus on lipid nanoparticles (LNPs) has demonstrated
63 effective mRNA delivery against COVID-19 in the clinic [3]. Thus, several preclinical
64 and clinical studies have been conducted to explore the effectiveness and safety of
65 mRNA cancer vaccines, either alone or in combination with chemotherapy or
66 immunotherapy [8]. In some clinical studies, mRNA-LNPs have demonstrated
67 considerable potential for cancer therapy [9, 10]. However, some studies on mRNA
68 cancer vaccines have either not shown any benefits or suggested harmful effects [11,
69 12]. Thus, further research is required to understand the interaction between mRNA-
70 LNPs and immune cells, and to optimize their efficacy and safety.

71 Accumulating evidence indicates that metabolic reprogramming hinders the
72 ability of immune cells to initiate an effective anti-tumor immune response [13]. Many
73 metabolites serve dual roles in metabolism and signaling, exerting direct or indirect
74 immunomodulatory effects. For instance, lactate, which accumulates in large quantities
75 within solid tumors, inhibits the proliferation and activation of cytotoxic T lymphocytes
76 (CTLs) and natural killer (NK) cells [14, 15]. It also supports the immunosuppressive
77 and tumor-promoting functions of $CD4^+$ $CD25^+$ $FOXP3^+$ regulatory T (Treg) cells [16,
78 17], and promotes the polarization of tumor-associated macrophages (TAMs) towards

an immunosuppressive M2-like phenotype, which is associated with poor disease outcomes [18, 19]. Moreover, immune cells- including T cells [20, 21], dendritic cells (DCs) [22], and Treg cells [23] take up fatty acids in a CD36-dependent manner. This process directly suppresses the function of CTLs and DCs, while promoting the expansion or activity of Treg cells. In summary, most metabolites, which are produced during the immune response, suppress immune cells such as T cells, DCs, and TAMs or activate immunosuppressive cells to influence the function of immune cells.

The mRNA encodes one or more proteins that are taken up by antigen-presenting cells (APCs), such as DCs and macrophages in lymph nodes, and presented on the surface by major histocompatibility complexes (MHCs) to induce anti-tumor immunity. Based on the direct or indirect impact of metabolites on the function or quantity of immune cells, we hypothesized that mRNA cancer vaccines, by inducing certain metabolites, would affect the function of immune cells. Thus, we analyzed the metabolome in the contralateral (non-draining; cLN) and ipsilateral (draining; iLN) lymph nodes (LNs) after subcutaneous injection of ovalbumin (OVA)-encoding mRNA-LNP (OVA-LNP). These findings indicated that the metabolite profile was different between iLNs and cLNs, and itaconate was the most highly upregulated metabolite in iLNs compared to cLNs. Itaconate is produced *via* the decarboxylation of the tricarboxylic acid (TCA)-derived cis-aconitate by aconitate decarboxylase (ACOD1), encoded by immune-response gene1 (*Irg1*, also known as *Acod1*) [24]. Previous studies have demonstrated that itaconate rapidly accumulates to high levels in myeloid cells during both infectious and sterile inflammatory conditions, where it plays

an immunomodulatory role in host innate immunity against infectious pathogens and non-infectious inflammatory processes [25]. However, whether itaconate affects mRNA vaccine efficacy remains unclear. In this study, we demonstrated that macrophage-derived itaconate in LNs diminishes antigen presentation of DCs, and T cell functions, which decreases the efficacy of mRNA cancer vaccines. Moreover, we designed the OVA&si-*Irg1*-LNP, which contained OVA mRNA and *Irg1* small interfering (si)RNA (si-*Irg1*), suppressed *Irg1* expression, and itaconate secretion *in vitro* and *in vivo*. More importantly, OVA&si-*Irg1*-LNP enhanced anti-tumor efficacy alone or combined with anti-programmed cell death-1 (anti-PD-1) antibody and showed good safety.

Materials and Methods

Mice

All animal experiments followed the guidelines of the Hubei Provincial Animal Care and Use Committee and the Animal Experimentation Ethics Committee of Huazhong University of Science and Technology. Female C57BL/6 mice aged 6-8 weeks were purchased from Hunan Slyke Jingda Laboratory Animal Co. LTD. The mice, including C57BL/6NJ-*Irg1*$^{em1(IMPC)}$J/J mice (also known as *Irg1*$^{-/-}$), Myeloid cell-specific *Irg1*-deficient (*Irg1*$^{f/f}$Lyz2^{Cre} mice), were bred and kept in specific-pathogen-free conditions at the Animal Center of Huazhong University of Science and Technology (HUST) in Wuhan, China. They were housed in a 12/12 h dark/light cycle environment with appropriate temperature, humidity, and adequate food and water.

Cell lines and cell culture

Mouse B16-F10 cells were acquired from the China Center for Type Culture Collection (Wuhan, China). The B16-F10-OVA cell line, which is stably transfected with ovalbumin, was kindly provided by prof. Bo Huang at the Chinese Academy of Medical Sciences and Peking Union Medical College, Beijing. The cells were grown in RPMI 1640 medium (11875093, Gibco) with 10% fetal bovine serum (FBS, 164210-50, Procell) and 1% penicillin/streptomycin (5140122, Gibco).

Metabolome analysis

Metabolome analysis was performed as described previously[26]. In brief, fresh iLNs and cLNs were collected from C57BL/6 mice at 24 h post-subcutaneous injection of OVA-LNP into the right flank. The LNs were homogenized in 70% methanol and centrifuged to obtain the supernatant. Next, acetonitrile (with 0.1% formic acid) and ultrapure water (with 0.1% formic acid) were added to the supernatant. After another round of centrifugation and filtration using a Waters ACQUITY UPLC HSS T3 Column, the concentrated filtrate was used for metabolite analysis.

Single-cell RNA sequencing

Three C57BL/6 mice received a subcutaneous injection of 5 μg of OVA-LNP. After 24 h, total iLNs and cLNs were collected and preserved in MACS Tissue Storage Solution (130-100-008, Miltenyi Biotec). The samples were then centrifuged at 50 g for 1 min at 4 °C and digested using a digestion solution (130-095-929, Miltenyi Biotec) in a 37 °C water bath for 45 min. After the incubation, the solution was filtered using a 40-μm cell strainer (CLS431750, Corning), and the red blood cells were removed with

red blood cell lysis buffer (11814389001, Roche). Finally, the single cells were resuspended in PBS with 0.01% Bovine serum albumin (A1933, Sigma) and subjected to single-cell RNA sequencing (scRNA-seq) using MobiDrop (Zhejiang) Co., Ltd., China.

In vitro stimulation of bone marrow-derived macrophages (BMDMs)

The bone marrow-derived cells from female C57BL/6 or *Irg1*$^{-/-}$ mice aged 6-10 weeks were collected, centrifuged for 5min, and depleted of red blood cells using a lysis buffer. Then, the femoral and tibial specimens were cultured in RPMI 1640 supplemented with 10% FBS and 20 ng/mL macrophage colony-stimulating factor (M-CSF, 576406, Biolegend). On day 6, the BMDMs were stimulated by 0.3 μg/mL OVA-LNP, and samples were collected at 0, 2, 4, 8, 12, and 24 h for quantitative reverse transcription-polymerase chain reaction (qRT-PCR) and flow cytometry. The supernatant at 24 h was collected as a conditioned medium.

Flow cytometry

In vitro, BMDMs and bone marrow-derived DCs (BMDCs) were collected and stained with antibodies at 4 ℃ for 30 min. And stained samples were acquired on the BD FACSymphony flow cytometer (BD Biosciences). Antibodies used in this study were listed in Supplementary Table 1.

In vivo, lymph nodes and tumors were harvested at the indicated time and then digested by 0.5 mg/mL hyaluronidase (HY-E70182, MedChemExpress) and 0.32 mg/mL collagenase V (HY-E70005E, MedChemExpress) for 45 min at 37 ℃ to make single-cell suspensions. Spleens and blood were depleted red blood cells with lysis

buffer to obtain the single cells. The single-cell suspension was blocked with anti-mouse CD16/32 (101320, Biolegend), and dead cells were stained with zombie NIR™ (423106, Biolegend) or Violet™ (423114, Biolegend) dye for 30 min. For cell membrane protein staining, cells were stained at 4 ℃ for 30 min. For intracellular cytokine staining, cells were incubated with a stimulation cocktail (1ug/mL Ionomycin (HY-13434, MedChemExpress), 1.5 μg/mL Monensin (HY-N4302, MedChemExpress), and 100 ng/mL Phorbol 12-myristate 13-acetate (HY-18739, MedChemExpress)) for 4 h or 2 μM OVA peptide (HY-P3715, MedChemExpress) for 16 h before cell surface and cytokine staining. Then, the cells were fixed, permeabilized, and stained with antibodies. All samples were analyzed using the BD FACSymphony flow cytometer from BD Biosciences. Antibodies used in this study were listed in Supplementary Table 1.

In vivo anti-tumor assay

For *in vivo* experiments, 6-8 weeks WT and *Irg1*$^{-/-}$ mice were used, and 3×10^5 B16-F10-OVA cells were implanted subcutaneously at the right flank on day 0. When the tumor volume reached 50mm^3, mice were randomly assigned to different groups and were administered the first dose of vaccination (5 μg OVA-LNP, si-*Irg1*-LNP, or OVA&si-*Irg1*-LNP) subcutaneously on day 7 and the booster dose on day 12. Mice with LNP without any mRNA are used as the control group. The mice were also administered InVivoMAb anti-mouse PD-1 (CD279, Clone: RMP1-14) (10 mg/kg) (BE0146, Bioxcell) intraperitoneally for the immune checkpoint blockade combined therapy on days 9, 14, and 17. To evaluate the effect of itaconate on tumors, 4-OI (50

mg/kg) was administered intraperitoneally daily from day 8 to day 14. The tumor volume (Vs) was monitored by a Vernier caliper and calculated as V=L (length) x W (Width)^2/2. Mice were sacrificed if the average diameter exceeded 15 mm or the tumor volumes exceeded 2000 mm^3.

qRT-PCR

Total RNA was extracted from cells or Tissues using RNAiso Plus Reagent (9109, Takara). After measurement for concentration and purity, RNA was reverse-transcribed into cDNA with HiScript III 1st Strand cDNA Synthesis Kit (+gDNA wiper) (R312-01, Vazyme). qRT-PCR was performed using ChamQ SYBR qPCR Master Mix (Q311-02, Vazyme). The primers used in the study are listed in Supplementary Table 2.

LC/MS analysis

The supernatant from BMDM or BMDC after stimulation with LNPs for 24 h, and the LNs 24 h after a subcutaneous injection of 5 μg LNPs was collected for LC/MS analysis.

Synthesis and formulation of mRNA-encapsulating LNPs

The LNPs were commercially synthesized by Rhegen Bio. Inc. First, OVA mRNA, si-Ctrl (Sequence-F: UUCUCCGAACGUGUCACGUTT; Sequence-R: ACGUGACACGUUCGGAGAATT), and si-*Irg1* (F: CAGGUUUACCAAUAUCUAAUU; R: UUAGAUAUUGGUAAACCUGGG) siRNA were diluted in 100 mM citrate buffer (pH 4.00) as the aqueous phase. At the same time, PEG-lipid (ALC-0519, 1.6%), cationic lipid (DSPC, 9%), cholesterol (42.7%), and phospholipid (ALC-0315, 46.3%) were dissolved in ethanol as the lipid

phase. The aqueous and lipid phases were mixed at a flow rate of 3: 1 using a Liposyn X Intelligent Lipid Nanoparticle Synthesis System (ED1001, Enoch (Shenzhen) Biotechnology Co). Next, the samples were transferred to a 100 kDa dialysis bag for overnight dialysis and subsequently concentrated using an ultrafiltration centrifuge tube. Finally, the LNPs underwent quality assurance testing for particle size, potential, and encapsulation rate.

***In vivo* safety evaluation**

To evaluate the safety of si-*Irg1*-LNP, OVA-LNP, and OVA&si-*Irg1*-LNP *in vivo*, the body weight was monitored every 3 days for 21 days after subcutaneous injection of 5 μg LNPs. Blood serum aspartate transaminase (AST), alanine aminotransferase (ALT), blood urea nitrogen (BUN), and creatinine (CR) levels were measured on days 7, 14, and 21. Additionally, heart, liver, spleen, lung, and kidney tissue samples were collected at the end of the experiment for histological and aminotransaminase analysis.

Statistical analysis

We used unpaired two-tailed *Student's* t-test and one-way ANOVA to compare two or more groups. Survival analysis was conducted with the log-rank test. All the results were analyzed using GraphPad Prism software and are presented as means ± SD or means ± SEM. The flow cytometry data was analyzed using FlowJo. Significant differences were indicated: ns = no significance, * $p < 0.05$, ** $p < 0.01$, *** $p < 0.001$.

Results

Metabolome analysis identified that itaconate suppresses T cell response to mRNA

cancer vaccine

Luciferase-LNPs were injected subcutaneously into mice, and organs were harvested for bioluminescence imaging after 24 h [27-29]. The iLN exhibited the highest bioluminescence signal (**Figure 1A**). Then, cLNs and iLNs were collected from mice that received a subcutaneous injection of 5 μg OVA-LNP, and the iLNs exhibited an activated status compared to the homeostatic cLNs (**Figure 1B**). Water-soluble metabolites analysis indicated that OVA-LNP strongly influenced the immunized LN metabolic landscape, with iLNs being distinct from cLNs (**Figure S1A**). In total, 219 metabolites were upregulated and 98 metabolites were downregulated after LNP injection, with itaconate being the most upregulated (**Figure 1C**). Pathway analysis of significantly different metabolites between iLNs and cLNs showed that pyrimidine, galactose, glycerophospholipid, and purine metabolism, and the TCA cycle were strongly associated with immune activation (**Figure S1B**). We analyzed the metabolites involved in the TCA cycle and observed that itaconate was upregulated by 44.6-fold. Additionally, its upstream and downstream metabolites, such as pyruvate, isocitrate, and α-ketoglutarate, were downregulated as expected (**Figure 1D-E**, **S1C-D**). Furthermore, we observed the downregulation of serine and glycine in iLNs compared to that in cLNs (**Figure S1E**). A previous study indicated that itaconate suppresses $CD8^+$ T cell proliferation and activation by hindering aspartate, serine, and glycine biosynthesis [30]. Thus, we speculated that itaconate induced by OVA-LNP may affect T cell function. Furthermore, *Irg1* expression and itaconate release were measured in various organs after OVA-LNP injection. The results demonstrateded that *Irg1* and

itaconate were predominantly upregulated mainly in iLNs (**Figure 1F-G**).

Because ACOD1 is a critical enzyme for itaconate production, we used *Irg1*-deficient mice (**Figure S1F**) to assess the effect of itaconate on tumors. To assess the impact of itaconate on the anti-tumor efficacy of OVA-LNP, we administered 4-octyl itaconate (4-OI), a cell-permeable derivative of itaconate, to B16-F10 tumor-bearing *Irg1*$^{-/-}$ mice. The results showed that 4-OI significantly increase tumor volume and weight after OVA-LNP treatment (**Figure S1F-H**). Meanwhile, 4-OI inhibited the expression of OVA and MHC I on DCs in iLNs (**Figure S1I-J**). Within the tumor microenvironment (TME), 4-OI reduced the frequencies of $CD8^+$ and $IFN\gamma^+$ $CD8^+$ T cells (**Figure S1K-L**), but had no significant impact on $CD4^+$, $Foxp3^+$ $CD4^+$ T cells, or myeloid-derived suppressor cells (MDSCs), including monocytic (M-MDSC) and granulocytic (M-MDSC) subsets (**Figure S1M-P**).

We next evaluate the T cell response to OVA-LNP in the *Irg1*-deficient mice (*Irg1*$^{-/-}$) (**Figure S2A**). First, *Irg1* and itaconate levels were measured in both WT and *Irg1*$^{-/-}$ mice. While *Irg1* deficiency did not affect the bioluminescence distribution (**Figure S2B**), *Irg1* expression and itaconate levels were significantly reduced in the peripheral blood and organs of *Irg1*$^{-/-}$ mice (**Figure S2C-E**). Subsequently, T cell function was assessed in the peripheral blood and spleen following the injection of 5 μg OVA-LNP (**Figure S2F**). The results indicated an increase in $CD8^+$ T cells in the blood after restimulation with 2 μM OVA peptide in the OVA-LNP immunized group (**Figure 1H**). Additionally, there was higher secretion of OVA sIgE and sIgG at days 14 and 21 (**Figure 1I, S2G**), and an elevated presence of interferon-γ ($IFN\gamma^+$) $CD8^+$ T cells in the

blood at day 21 (**Figure 1J**) compared to the control group. Notably, *Irg1* deficiency further enhanced these effects (**Figure 1H-J**). We also examined $CD4^+$ and $CD8^+$ T cells in the spleens of the control and OVA-LNP immunized mice. The percentages of $CD4^+$ and $CD8^+$ T cells among $CD3^+$ T cells were unaffected by OVA peptide stimulation (**Figure 1K, M**). However, there was a significant increase in $IFN\gamma^+$ $CD4^+$ and $IFN\gamma^+$ $CD8^+$ T cells in the OVA-LNP immunized group, and this increase was even more pronounced in mice with *Irg1* deficiency (**Figure 1L, N**, **S2H**). Furthermore, when spleen cells were co-cultured with B16-F10-OVA cells at an effector: target (E: T) ratio of 25: 1, the most robust cytotoxicity was observed in the OVA-LNP immunized *Irg1*-deficient group (**Figure 1O**). These data indicate that *Irg1* affects T cells following OVA-LNP immunization.

OVA-LNP-induced itaconate derives from macrophages in iLNs

Itaconate is produced by myeloid cells, significantly activated macrophages, in response to inflammatory stimuli and cellular stresses. Recent studies have shown that *Irg1* is highly expressed in tumor-infiltration neutrophils (TINs), which constrains breast cancer metastasis [31]. Thus, we investigated which cell type upregulated *Irg1* expression induced by OVA-LNP in iLNs. We dissociated iLNs and cLNs according to the procedure shown in Figure 1A and subjected them to scRNA-seq. The seven identified clusters were visualized using uniform manifold approximation and projection for reduction (UMAP) algorithm based on gene expression, including $CD8^+$ T cell, $CD4^+$ T cell, epithelium, DC, macrophage, B cell, and fibroblast (**Figure 2A**). The data revealed that *Irg1* was expressed in seven clusters and was highly expressed

in macrophages (**Figure 2B**). Compared with cLNs, *Irg1* was significantly upregulated in iLNs, particularly in macrophages (**Figure 2C-D**). Additionally, we subcutaneously injected enhanced green fluorescent protein (eGFP)-LNP into C57BL/6 mice and obtained iLNs after 24 h. The percentage of $eGFP^+$ immune cells was detected using flow cytometry, and the data indicated that macrophages were the primary $eGFP^+$ cells among T cells, B cells, NK cells, and DCs (**Figure 2E**), which is consistent with the scRNA-seq results.

To confirm the *Irg1*-derived cell type, we inoculated 3×10^5 B16-F10-OVA tumor cells subcutaneously into $Irg1^{f/f}$Lyz2 $^{cre+}$ and $Irg1^{f/f}$Lyz2 $^{cre-}$ mice, which *Irg1* deficiency specifically in macrophages (**Figure S3A**), and treated them with OVA-LNP on day 7 when tumor volume reached to $50mm^3$, followed by a boost dose on day 12. The tumor volume was monitored every 3 days after treatment. The results indicated that a deficiency in *Irg1*, specifically in macrophages, enhanced the anti-tumor effectiveness of the mRNA cancer vaccines (**Figure 2F-G**). Flow cytometry results suggested that a deficiency of *Irg1* in macrophages elevated the number of $CD45^+$ immune cells, macrophages, and DCs within the TME (**Figure 2H-J**). In addition, T cell function was significantly increased after OVA-LNP treatment in *the* $Irg1^{f/f}$Lyz2 $^{cre+}$ group, presented as upregulation of $IFN\gamma^+$ $CD8^+$ T cells (**Figure 2K**). Furthermore, clodronate liposomes (Clo) were administered to deplete macrophages prior to OVA-LNP injection. Flow cytometry analysis confirmed successful macrophage depletion in the peripheral blood (**Figure S3B**). Clo treatment reduced *Irg1* expression and itaconate levels in the peripheral blood and organs, which were otherwise elevated by OVA-LNP stimulation.

(**Figure 2L-N**). These results confirmed that itaconate induced by OVA-LNP was derived from macrophages and affected anti-tumor efficacy *via* immune cells.

Irg1 deletion promotes pro-inflammatory activation of macrophages

Macrophages that deplete *Irg1* are polarized towards a pro-inflammatory state after lipopolysaccharide (LPS) and IFNγ stimulation, leading to enhanced tumor suppression and increased survival [32]. First, we analyzed scRNA-seq and found that OVA-LNP induces pro-inflammatory and antigen-presentation pathway enrichment of macrophages in iLNs compared to that in cLNs (**Figure S4A**). To confirm the role of *Irg1* in macrophage activation, we isolated BMDMs from C57BL/6 (WT) and *Irg1*$^{-/-}$ mice. After stimulation with OVA-LNP for 24 h, pro-inflammatory activation of BMDMs was detected using flow cytometry. The results indicated a higher upregulation of CD80, CD86, MHC I, MHC II, and CCR7 expression in *Irg1*-deleted BMDMs than WT BMDMs following treatment with OVA-LNP (**Figure 3A-E**). Pro-inflammatory genes such as *Il1β, Il6, Il23α, Cxcl9, Cxcl11*, and *Ccr7* were detected at 2, 4, 8, and 12 h post-OVA-LNP stimulation using qRT-PCR. We observed an increase in the expression of these genes in *Irg1*-deleted BMDMs, especially after 12 h of stimulation (**Figure 3F**). OVA mRNA expression increased significantly at 2 h and remained elevated up to 12 h, and there was no significant difference between WT and *Irg1*$^{-/-}$ BMDMs (**Figure S4B**). Additionally, *Irg1* was upregulated at 2 h and notably increased at 12 h in WT BMDMs, whereas no expression was observed in *Irg1*$^{-/-}$ BMDMs (**Figure S4C**). Additionally, we encapsulated LNPs with another mRNA, eGFP, and found that eGFP-LNP treatment similarly induced *Irg1* upregulation and

itaconate release without affecting the viability or proliferation of BMDMs (**Figure S4D-G**). These data demonstrated that *Irg1* plays a critical role in regulating the pro-inflammatory activation of macrophages without affecting OVA expression following OVA-LNP stimulation *in vitro*.

To investigate the potential mechanisms of *Irg1* upregulation in macrophages, we analyzed the Kyoto Encyclopedia of Genes and Genomes (KEGG) enrichment pathways of macrophages in iLNs compared to those in cLNs. The data showed that except activation pathways, such as the MAPK, JAK-STAT signaling pathways, and cytokine-cytokine receptor interaction, pattern recognition receptors (PRRs) that participate in vaccine adjuvant responses, such as TOLL-like receptors (TLR) and NOD-like receptors (NLR) [33], were more enriched in iLNs than in cLNs (**Figure 3G**). Studies have reported that mRNA and certain cationic lipids possess intrinsic adjuvant activity and potent immunostimulatory properties, enabling them to be recognized by PRRs of the innate immune system [8, 34, 35]. Therefore, we incubated OVA-LNP-treated macrophages with the TLR inhibitor (MYD88i), NOD1 inhibitor (NOD1i), and another essential PRR-RIG-1-like receptor (RLR) inhibitor (RIG1i), although did not enrich in the KEGG enrichment pathway. We found that all inhibitors suppress OVA-LNP-induced *Irg1* expression, and combining two inhibitors enhanced this effect, with three inhibitors showing the most potent inhibition (**Figure 3H**). PRRs induce gene expression via phosphorylated activation of interferon regulatory Factor 3 (IRF3), nuclear factor kappa-B (NF-κB), and c-JUN. Thus, we detected IRG1, IRF3, NF-κB p65 and JUN, and their phosphorylation level by western blotting analysis. The results

showed that OVA-LNP induced increased IRG1 expression and IRF3, NF-κB p65 and JUN activation, and MYD88i, NOD1i, and RIG1i inhibited this effect (**Figure 3I**). These data indicated that OVA-LNP led to an increase in *Irg1* expression in macrophages *via* multiple PRR pathways.

Macrophage-derived itaconate suppresses antigen presentation of DC in LNs

Plasmodium-induced itaconate restrains monocyte-derived DCs by disrupting the mitochondria, leading to the release of nucleic acids, which induces PD-L1 expression in DCs, and then impairs $CD8^+$ T cell activation [36]. DCs are critical APCs after mRNA-LNP stimulation and are activated to present antigens, express co-stimulatory molecules, and transition from innate to adaptive immunity [33]. Thus, we were curious to determine whether itaconate affects the function of DCs after OVA-LNP treatment. We detected OVA and *Irg1* expression in BMDMs and BMDCs after stimulation with OVA-LNP for 12 h. The results indicated that OVA expression was significantly higher upregulated in BMDMs than in BMDCs (**Figure 4A**), and *Irg1* expression was markedly increased in BMDMs after OVA-LNP treatment, with no significant change observed in BMDCs (**Figure 4B**). Itaconate secretion was detected in the supernatant of both BMDMs and BMDCs at 24 h using liquid chromatography-mass spectrometry (LC/MS) analysis. We observed a much more significant increase of itaconate in BMDMs rather than in BMDCs, consistent with *Irg1* expression (**Figure 4C**). These findings suggest that OVA-LNP-induced *Irg1* and itaconate are primarily derived from macrophages, rather than DCs. BMDMs from WT and $Irg1^{-/-}$ mice were used to collect conditioned medium (CM) after OVA-LNP treatment for 24 h, and then BMDCs were

cultured using this CM (**Figure S5A**). We measured itaconate in the supernatants of WT and *Irg1*$^{-/-}$ BMDMs and observed high itaconate levels secreted in OVA-LNP-treated WT BMDMs but not in *Irg1*$^{-/-}$ BMDMs (**Figure 4D**). After culturing in the CM for 24 h, we found that CM derived from *Irg1*-depleted BMDMs upregulated CD80, CD86, and MHC II of BMDCs compared to WT BMDMs (**Figure 4E-G**, **S5B**). In addition, *Il1β, Il8, Cxcl9, Cxcl10,* and *Ccr7* mRNA expression were measured, and were considerably higher in BMDCs treated with *Irg1*-depleted BMDMs than WT BMDMs (**Figure 4H**). We next treated BMDCs with 4-OI *in vitro*. The results demonstrated that while 4-OI did not affect BMDC viability, it significantly suppressed their proliferation (Figure S5C-D). To rule out the influence of pro-inflammatory cytokines released by BMDMs, BMDCs were supplemented with 4-OI following Irg1$^{-/-}$-CM treatment. This approach revealed that 4-OI treatment reduced the expression of OVA, MHC I, and MHC II in BMDCs (**Figure S5E-G)**.

To confirm the role of itaconate in the function of DCs *in vivo*, we isolated BMDCs and exposed them to OVA peptide and 4-OI. We then transferred these BMDCs to mice bearing B16-F10-OVA tumor cells at day 5. The injection of DCs significantly reduced tumor growth compared to that in the control group, and this effect was inhibited by 4-OI (**Figure 4I-K**). Within the TME, the transfer of DCs led to a significant increase in immune cells and CD3$^+$, CD4$^+$, and CD8$^+$ T cells (**Figure 4L**). This increase was accompanied by an increase in IFNγ$^+$ CD4$^+$ and IFNγ$^+$ CD8$^+$ T cells (**Figure 4M-N**). Furthermore, 4-OI diminished the activation of the TME by DCs (**Figure 4L-N**). These results indicate that itaconate produced by macrophages in response to OVA-LNP

inhibits DC function.

Encapsulating si-*Irg1* with OVA mRNA in LNP efficiently decreases itaconate and enhances APCs and T cell function *in vitro* and *in vivo*

As mentioned, itaconate inhibits tumor suppression and reduces the immune response to mRNA cancer vaccines. To reduce the production of itaconate from macrophages, we synthesized si-*Irg1* siRNA and encapsulated it along with OVA mRNA into the same LNP (OVA&si-*Irg1*-LNP) to deliver exogenous mRNA and siRNA to macrophages in the LNs (**Figure 5A**). The OVA&si-*Irg1*-LNP exhibited a uniform spherical shape with a "membrane-core" structure, as observed by cryo-transmission electron microscopy (cryo-TEM) (**Figure 5B**). We characterized the OVA-LNP and OVA&si-*Irg1*-LNP formulations, measuring particle sizes of approximately 80–100 nm using dynamic light scattering (DLS) (**Figure 5C**). The zeta potentials of these LNPs ranged from -15 to +15 (**Figure 5D**). Both formulations exhibited high encapsulation efficiency (≥ 90%) with mRNA concentrations of ≥ 0.100 mg/mL (Figure S6A). To serve as a control for si-*Irg1*, we designed si-Ctrl and encapsulated it in OVA&si-Ctrl-LNP. No significant differences were observed between OVA-LNP and OVA&si-Ctrl-LNP in promoting *Irg1* and itaconate upregulation (**Figure S6B-C**). Additionally, LNP stimulation had no noticeable impact on BMDM viability or proliferation (**Figure S6D-E**). In this study, we assessed the effect of siRNAs on BMDMs. Our findings revealed that *Irg1* expression was significantly reduced with OVA&si-*Irg1*-LNP compared to that with OVA-LNP after 8

h, whereas the expression of OVA was unaffected (**Figure 5E**, **S6F**). Additionally, itaconate levels in the supernatant were much lower in OVA&si-*Irg1*-LNP than in OVA-LNP (**Figure 5F**). Additionally, we measured OVA and *Irg1* expression in the iLNs after subcutaneous injection. Our findings indicated that OVA&si-*Irg1*-LNP effectively downregulated *Irg1* without affecting OVA expression at 24 and 48 h (**Figure 5G**, **S6G**). Furthermore, itaconate levels in the LNs were reduced following OVA&si-*Irg1*-LNP injection (**Figure 5H**). We also measured the expression level of OVA and *Irg1* in the spleen. The data revealed that OVA was upregulated in both groups at 24 and 48h, whereas *Irg1* was downregulated at 48 h. However, the expression levels of both OVA and *Irg1* were considerably lower than those in the LNs (**Figure S6H-I**). Therefore, the reduction of itaconate levels using OVA&si-*Irg1*-LNP is a promising strategy for improving the efficacy of cancer vaccines.

Next, we certified its effects on APCs and T cells. We isolated BMDMs, treated them with OVA-LNP and OVA&si-*Irg1*-LNP, and determined their activation states using flow cytometry. The data showed that OVA&si-*Irg1*-LNP upregulated CD80, CD86, MHC I, and H-2^b bound to SIINFEKL compared with OVA-LNP (**Figure 5I-L**). Next, LNPs were injected subcutaneously into mice, iLNs at 24 h, spleens on day 21, and blood serum on days 14 and 21 were collected. The levels of CD86 and H-2^b bound to SIINFEKL of macrophages and DCs in the iLNs were upregulated in the OVA-LNP group compared to those in the control group. Moreover, these levels were higher in the OVA&si-*Irg1*-LNP group in both macrophages (**Figure 5M-N**) and DCs (**Figure 5O-P**). Spleen cells were obtained and pulsed with OVA peptide for 16 h, followed by

monensin treatment for 4 h. IFNγ and granzyme B (Gzmb) levels were detected by flow cytometry. The data showed that OVA&si-*Irg1*-LNP increased IFNγ$^+$ Gzmb$^+$ T cells of CD4$^+$ and CD8$^+$ T cells compared to OVA-LNP (**Figure 5Q-R**). In addition, the OVA sIgE antibody levels increased on days 14 and 21 in both groups compared to those in the control group, with significantly higher levels observed in the OVA&si-*Irg1*-LNP group on day 21 (**Figure 5S-T**). These data demonstrate that targeting *Irg1* with LNPs efficiently enhances the function of APCs and T cells *in vitro* and *in vivo*.

Treatment with OVA&si-*Irg1*-LNP promotes therapeutic efficacy and remodels the TME in the B16-F10 melanoma mouse model

mRNA cancer vaccines have shown great promise in preclinical studies and have been tested in clinical trials. OVA&si-*Irg1*-LNP have been demonstrated to enhance APC and T cell functions. To confirm the anti-tumor therapeutic effect, we established a B16-F10-OVA tumor model, and 5 μg OVA-LNP, si-*Irg1*-LNP, or OVA&si-*Irg1*-LNP was administered subcutaneously on day 7 when the tumor volume reached 50mm^3, and a boost dose was given on day 12 (**Figure 6A**). Control mice displayed rapid tumor growth, which was slightly inhibited by si-*Irg1*-LNP. However, OVA-LNP significantly suppressed tumor growth, and OVA&si-*Irg1*-LNP inhibited tumor growth more effectively than OVA-LNP (**Figure 6B-C**). The survival rate was consistent with tumor growth (**Figure 6D**).

As previously mentioned, OVA&si-*Irg1*-LNP significantly enhanced the activation and antigen presentation of macrophages and DCs in the iLNs, as well as the anti-tumor functions of T cells in the spleen. At the end of the therapeutic tumor model,

475 we evaluated the infiltration of macrophages, DCs, and T cells within the TME using
476 flow cytometry (**Figure S7A-B**). The results indicated that OVA&si-*Irg1*-LNP
477 significantly increased the number of immune cells, myeloid cells, DCs, and
478 macrophages (**Figure 6E-H**) within the TME compared to OVA-LNP. Additionally,
479 CD86 expression in macrophages was slightly but not significantly upregulated (**Figure**
480 **6I**). T cells play a critical role in anti-tumor efficacy, and we found that the proportion
481 of $CD3^+$ and $CD4^+$ T cells was slightly increased in the OVA&si-*Irg1*-LNP group
482 compared to that in the OVA-LNP group (**Figure 6J-K**). However, $CD8^+$, $IFN\gamma^+$ $CD4^+$,
483 and $IFN\gamma^+$ $CD8^+$ T cells were significantly increased by OVA&si-*Irg1*-LNP (**Figure 6L-**
484 **N**). We administered LNPs at two doses, and one month later, established the B16-F10
485 tumor mouse model to evaluate their protective efficacy (**Figure S7C**). The results
486 demonstrated that OVA&si-*Irg1*-LNP was more effective in inhibiting tumor growth
487 and prolonging mouse survival compared to controls (**Figure S7D-E**). Body weight
488 was monitored after a single subcutaneous injection to investigate the safety of OVA-
489 LNP, si-*Irg1*-LNP, and OVA&si-*Irg1*-LNP *in vivo*. Body weights were unchanged
490 compared with those in the control group (**Figure S8A**). Alanine transaminase (ALT)
491 and aspartate transaminase (AST), used in liver function tests, and blood urea nitrogen
492 (BUN) and creatinine (CR), used in kidney function tests, were measured using
493 biochemical assays on days 7, 14, and 21. All these markers were below normal levels
494 and with no obvious changes in the four groups (**Figure S8B-E**). After vaccination, the
495 heart, liver, spleen, lung, and kidney tissues were collected, and hematoxylin and eosin
496 (H&E) staining was performed. The results showed no apparent changes in the main

organs, indicating that the LNPs were safe *in vivo* (**Figure S8F**).

In summary, OVA&si-*Irg1*-LNP treatment induced enhanced anti-tumor effects, increased myeloid and T cell infiltration into the TME, and demonstrated good safety. These data indicate that targeting *Irg1* has excellent potential for tumor therapy.

Targeting itaconate enhances the anti-tumor activity of cancer vaccine in combination with anti-PD-1 antibody *in vivo*

Combining cancer vaccines with anti-PD-1 antibodies is an effective strategy for improving the therapeutic effects against cancer. We injected B16-F10-OVA cells subcutaneously on day 0, administered vaccines on days 7 and 12, and anti-PD-1 antibodies on days 9, 14, and 17 (**Figure 7A**). We observed that a combined therapeutic strategy enhanced the anti-tumor activity of the anti-PD-1 antibody. Combining OVA&si-*Irg1*-LNP with anti-PD-1 antibodies yielded the most effective therapeutic results (**Figure 7B-D**). Immune cells, such as DCs, macrophages, and $CD8^+$ T cells, were measured using immunofluorescence. The data revealed that both LNPs and anti-PD-1 antibodies, either alone or in combination, increased the infiltration of immune cells compared with the untreated group. In the combined treatment groups, a higher proportion of macrophages and $CD8^+$ T cells were present within the TME compared to treatment with LNPs alone. Importantly, OVA&si-*Irg1*-LNP combined with the anti-PD-1 antibody led to significantly more DC infiltration into the TME than the other treatments (**Figure 7E**). These results demonstrated that combining a cancer vaccine with an anti-PD-1 antibody improved anti-tumor efficacy, and targeting *Irg1* enhanced

519 the combined therapy.

520

521 **Discussion**

522 mRNA possesses intrinsic adjuvant activity and can be recognized by specific
523 PRRs of the innate immune system, boosting the full activation of adaptive immunity.
524 The immune system displays potent immunostimulatory capabilities, activating
525 immune responses while simultaneously initiating negative feedback mechanisms to
526 prevent excessive or prolonged activation. This regulation involves various pathways,
527 including glucocorticoids, which not only induce an inflammatory state but also trigger
528 a systemic increase in itaconate, contributing to its anti-inflammatory effects [37].
529 Moreover, D-2-hydroxyglutarate exhibits anti-inflammatory effects and has been
530 shown to accumulate in macrophages following TLR activation [38]. IFNγ, primarily
531 produced by $CD8^+$ cytotoxic T lymphocytes, plays a critical role in antitumor immunity.
532 However, studies have shown that IFNγ can also upregulate PD-L1 expression on tumor
533 cells, thereby facilitating tumor immune evasion and promoting tumor progression[39-
534 42]. In this study, we observed significant changes in metabolites following stimulation
535 with an mRNA cancer vaccine, with itaconate being the most upregulated metabolite.
536 Itaconate suppressed antigen presentation by DCs and decreased the efficacy of mRNA
537 cancer vaccines. These data demonstrated that changes in the metabolic environment
538 of LNs play a critical role in the immune response to cancer vaccines. Recent studies
539 have shown that exposure to a high-fat diet limits T cell maturation in the memory
540 compartment during influenza vaccination, corresponding to changes in systemic

obesity-related biomarkers such as leptin and adiponectin [43]. patients with melanoma who received DC vaccines showed that clinical outcomes correlate with the DC metabolic profile, and that metabolism is related to the immune phenotype [44]. These studies suggest that alterations in metabolite profiles are correlated with vaccine efficacy and that targeting abnormal metabolites may improve the immune response to vaccines. However, alterations in metabolites and their roles in mRNA cancer vaccines have not yet been studied.

Itaconate binds to diverse proteins intracellularly, regulating metabolism, oxidative responses, epigenetic modifications, and gene expression, while also signaling extracellularly through G protein-coupled receptors [25, 45]. Itaconate is an anti-inflammatory metabolite in inflammatory diseases, but it also promotes tumorigenesis and inhibits anti-tumor immunotherapy by impairing immune cell function [46, 47]. Recent studies have identified SLC13A3 as an importer of itaconate, with SLC13A3-mediated uptake contributing to tumor immune evasion, resistance to ferroptosis, and hepatic antibacterial innate immunity [48-50]. In this study, we found that macrophage-derived itaconate suppresses the activation and antigen-presentation of DCs in iLNs. However, whether itaconate induced by mRNA-LNPs in iLNs is taken up by DCs remains to be further investigated. The same metabolite can have opposing effects on tumor cells and immune cells. Itaconate, produced by polymorphonuclear myeloid-derived suppressor cells (PMN-MDSCs), myeloid cells such as monocytes and macrophages, or tumor-infiltrating neutrophils, promotes tumor progression by suppressing $CD8^+$ T cell proliferation and function [30, 31]. However, a recent study

563 revealed that tumor-intrinsic itaconate production can enhance $CD8^+$ T cell infiltration
564 and activation by modulating tumor immunogenicity [51]. These findings suggest that
565 the same metabolite may exert divergent effects—suppressive or stimulatory—
566 depending on whether it acts intracellularly within tumor cells or extracellularly on
567 neighboring immune cells. In this study, we demonstrated that OVA-LNP-induced
568 itaconate, which is derived from macrophages in iLNs, reduces the immune response
569 to cancer vaccines by impairing antigen presentation and the activation of DCs and
570 inhibiting the anti-tumor function of T cells. Targeting itaconate with si-*Irg1* effectively
571 reduced itaconate levels in iLNs and improved the anti-tumor efficacy of the mRNA
572 cancer vaccine. Currently, *Irg1* depletion in mice has been used to target itaconate in
573 cancer immunotherapy [30, 32, 52-54]. However, exogenous depletion has not been
574 investigated. We propose a new strategy for targeting itaconate in LNs, which enhances
575 the effectiveness of cancer vaccines with good safety. This may provide a new strategy
576 for improving the efficacy of mRNA cancer vaccines.

577 Our study focused on itaconate induction by mRNA cancer vaccines and its
578 inhibitory functions, and we proposed a strategy to enhance tumor suppression by
579 mRNA cancer vaccines. In the future, it will be important to investigate whether
580 itaconate production depends on the type of vaccine used, such as peptide- or DNA-
581 based vaccines. We used OVA as a model antigen, which is specifically expressed in
582 stably transfected B16-F10-OVA cell lines. Further research is required to investigate
583 the role of itaconate in other tumor-associated and tumor-specific antigens (like HER2,
584 KRAS mutations). Nonetheless, identifying itaconate and its immunosuppressive

biological functions in mRNA cancer vaccines, and providing a strategy to inhibit its inhibitory functions offer the possibility of enhancing the effectiveness of cancer immunotherapies.

Conclusion

Our results indicate that itaconate is the most upregulated metabolite in activated iLNs compared to that in homeostatic cLNs after OVA-LNP stimulation. Depletion of *Irg1* improved T-cell mediated tumor killing and antibody production by B cells. We demonstrated that itaconate induced by OVA-LNP was mainly derived from macrophages in the LNs, which is consistent with previous tumor studies [30, 54, 55]. We observed an enhanced pro-inflammatory state in macrophages after *Irg1* depletion and demonstrated that OVA-LNP induced *Irg1* expression *via* multiple PPR pathways. We also demonstrated that DCs are the target cells of macrophage-derived itaconate in the LNs. To enhance the efficacy of mRNA cancer vaccines, we designed OVA&si-*Irg1*-LNP, which encapsulated OVA and si-*Irg1* into the same LNP. The expression of *Irg1* and itaconate was effectively downregulated in BMDMs and LNs, leading to an enhanced pro-inflammatory state in BMDM and heightened macrophage, DC, and T cell responses to cancer vaccines. Importantly, OVA&si-*Irg1*-LNP demonstrated potent anti-tumor efficacy when used alone or in combination with an anti-PD-1 antibody and also increased the infiltration of immune cells, including DCs, macrophages, and T cells. In addition, we observed good safety of OVA&si-*Irg1*-LNP. We found that macrophage-derived itaconate impaired the efficacy of cancer vaccines, and

607 demonstrated a method to circumvent this activity, which may provide a strategy to
608 improve the therapeutic efficacy of mRNA cancer vaccines.
609
610 **Acknowledgments**
611 **Funding**
612 This work was supported by grants from the National Natural Science Foundation of
613 China (Grant No. 82303715, 82330085, 82272901, 82373235), the China Postdoctoral
614 Science Foundation (2023M731218), and the Hubei Key Laboratory of Precision
615 Radiation Oncology (jzfs007).
616 **Author Contributors**
617 K.Y.Y. and C.W. conceived and supervised the project. C.W. and W.W.W. designed the
618 experiments. W.W.W., X.Y., Y.S.C., and M.J.C. performed all experiments. Y.D. and
619 M.Y.S. contributed to animal experiments. Y.J.S., J.S.M., Y.H., Y.L., and Q.L.
620 contributed to technical and material support. J.C.W., Y.J.W., Z.S.C., and Z.Y.Z.
621 contributed to Western blotting analysis. Y.Y. performed the bioinformatic analysis. All
622 authors analyzed and discussed the data. and W.W.W. wrote the paper. K.Y.Y, C.W.,
623 Y.Q., Z.J.Z., B.W., H.B.Z, and L.W. reviewed and revised the manuscript.
624 **Data availability**
625 The data supporting this study's findings are available from the corresponding authors
626 upon reasonable request, Kunyu Yang (yangkunyu@hust.edu.cn), and Chao Wan
627 (wanc@hust.edu.cn).
628 **Ethics approval**

All animal experiments were approved by the Committee and the Animal Experimentation Ethics Committee of Huazhong University of Science and Technology (IACUC number: 4059).

Competing Interests

The authors have declared that no competing interest exists.

References

1. Conry RM, LoBuglio AF, Wright M, Sumerel L, Pike MJ, Johanning F, et al. Characterization of a messenger RNA polynucleotide vaccine. Cancer Res. 1995; 55: 1397-400.
2. Sahin U, Karikó K, Türeci Ö. mRNA-based therapeutics-developing a new class of drugs. Nat Rev Drug Discov. 2014; 13: 759-80.
3. Polack FP, Thomas SJ, Kitchin N, Absalon J, Gurtman A, Lockhart S, et al. Safety and efficacy of the BNT162b2 mRNA Covid-19 vaccine. N Engl J Med. 2020; 383: 2603-15.
4. Qu P, Faraone JN, Evans JP, Zheng YM, Yu L, Ma Q, et al. Durability of booster mRNA vaccine against SARS-CoV-2 BA.2.12.1, BA.4, and BA.5 subvariants. N Engl J Med. 2022; 387: 1329-31.
5. Karikó K, Buckstein M, Ni H, Weissman D. Suppression of RNA recognition by Toll-like receptors: the impact of nucleoside modification and the evolutionary origin of RNA. Immunity. 2005; 23: 165-75.
6. Huang X, Kong N, Zhang X, Cao Y, Langer R, Tao W. The landscape of mRNA nanomedicine. Nat Med. 2022; 28: 2273-87.
7. Xiong Q, Lee GY, Ding J, Li W, Shi J. Biomedical applications of mRNA nanomedicine. Nano Res. 2018; 11: 5281-309.
8. Liu C, Shi Q, Huang X, Koo S, Kong N, Tao W. mRNA-based cancer therapeutics. Nat Rev Cancer. 2023; 23: 526-43.
9. Weber JS, Carlino MS, Khattak A, Meniawy T, Ansstas G, Taylor MH, et al. Individualised neoantigen therapy mRNA-4157 (V940) plus pembrolizumab versus pembrolizumab monotherapy in resected melanoma (KEYNOTE-942): a randomised, phase 2b study. The Lancet. 2024; 403: 632-44.
10. Wang X, Wang W, Zou S, Xu Z, Cao D, Zhang S, et al. Combination therapy of KRAS G12V mRNA vaccine and pembrolizumab: clinical benefit in patients with advanced solid tumors. Cell Res. 2024; 34: 661-4.
11. Vansteenkiste JF, Cho BC, Vanakesa T, De Pas T, Zielinski M, Kim MS, et al. Efficacy of the MAGE-A3 cancer immunotherapeutic as adjuvant therapy in patients with resected MAGE-A3-positive non-small-cell lung cancer (MAGRIT): a randomised, double-blind, placebo-controlled, phase 3 trial. Lancet Oncol. 2016; 17: 822-35.

12. Koch SD, Hong H, Feyerabend S, Retz M, Kuebler H, Heidenreich A, et al. A randomized, double-blind, placebo-controlled, Phase I/II trial of RNActive®-vaccine cv9104 in patients with metastatic castrate-refractory prostate cancer (mcrpc): first results of the Phase I part. J Immunother Cancer. 2014; 2: 85.
13. Kroemer G, Chan TA, Eggermont AMM, Galluzzi L. Immunosurveillance in clinical cancer management. CA Cancer J Clin. 2024; 74: 187-202.
14. Elia I, Rowe JH, Johnson S, Joshi S, Notarangelo G, Kurmi K, et al. Tumor cells dictate anti-tumor immune responses by altering pyruvate utilization and succinate signaling in CD8(+) T cells. Cell Metab. 2022; 34: 1137-50.
15. Ma J, Tang L, Tan Y, Xiao J, Wei K, Zhang X, et al. Lithium carbonate revitalizes tumor-reactive CD8(+) T cells by shunting lactic acid into mitochondria. Nat Immunol. 2024; 25: 552-61.
16. Kumagai S, Koyama S, Itahashi K, Tanegashima T, Lin YT, Togashi Y, et al. Lactic acid promotes PD-1 expression in regulatory T cells in highly glycolytic tumor microenvironments. Cancer Cell. 2022; 40: 201-18.
17. Watson MJ, Vignali PDA, Mullett SJ, Overacre-Delgoffe AE, Peralta RM, Grebinoski S, et al. Metabolic support of tumour-infiltrating regulatory T cells by lactic acid. Nature. 2021; 591: 645-51.
18. Chen P, Zuo H, Xiong H, Kolar MJ, Chu Q, Saghatelian A, et al. Gpr132 sensing of lactate mediates tumor-macrophage interplay to promote breast cancer metastasis. Proc Natl Acad Sci U S A. 2017; 114: 580-5.
19. Qian Y, Galan-Cobo A, Guijarro I, Dang M, Molkentine D, Poteete A, et al. MCT4-dependent lactate secretion suppresses antitumor immunity in LKB1-deficient lung adenocarcinoma. Cancer Cell. 2023; 41: 1363-80.
20. Xu S, Chaudhary O, Rodríguez-Morales P, Sun X, Chen D, Zappasodi R, et al. Uptake of oxidized lipids by the scavenger receptor CD36 promotes lipid peroxidation and dysfunction in CD8(+) T cells in tumors. Immunity. 2021; 54: 1561-77.
21. Ma X, Xiao L, Liu L, Ye L, Su P, Bi E, et al. CD36-mediated ferroptosis dampens intratumoral CD8(+) T cell effector function and impairs their antitumor ability. Cell Metab. 2021; 33: 1001-12.
22. Jiang L, Fang X, Wang H, Li D, Wang X. Ovarian Cancer-Intrinsic Fatty Acid Synthase Prevents Anti-tumor Immunity by Disrupting Tumor-Infiltrating Dendritic Cells. Front Immunol. 2018; 9: 2927.
23. Wang H, Franco F, Tsui YC, Xie X, Trefny MP, Zappasodi R, et al. CD36-mediated metabolic adaptation supports regulatory T cell survival and function in tumors. Nat Immunol. 2020; 21: 298-308.
24. Michelucci A, Cordes T, Ghelfi J, Pailot A, Reiling N, Goldmann O, et al. Immune-responsive gene 1 protein links metabolism to immunity by catalyzing itaconic acid production. Proc Natl Acad Sci U S A. 2013; 110: 7820-5.
25. Ye D, Wang P, Chen L-L, Guan K-L, Xiong Y. Itaconate in host inflammation and defense. Trends Endocrinol Metab. 2024; 35: 586-606.
26. Miyajima M, Zhang B, Sugiura Y, Sonomura K, Guerrini MM, Tsutsui Y, et al. Metabolic shift induced by systemic activation of T cells in PD-1-deficient mice perturbs brain monoamines and emotional behavior. Nat Immunol. 2017; 18: 1342-52.
27. Qiu K, Duan X, Mao M, Song Y, Rao Y, Cheng D, et al. mRNA-LNP vaccination-based immunotherapy augments CD8+ T cell responses against HPV-positive oropharyngeal cancer.

NPJ Vaccines. 2023; 8.
28. Wang Y, Zhang L, Xu Z, Miao L, Huang L. mRNA vaccine with antigen-specific checkpoint blockade induces an enhanced immune response against established melanoma. Mol Ther. 2018; 26: 420-34.
29. Oberli MA, Reichmuth AM, Dorkin JR, Mitchell MJ, Fenton OS, Jaklenec A, et al. Lipid nanoparticle assisted mRNA delivery for potent cancer immunotherapy. Nano Lett. 2017; 17: 1326-35.
30. Zhao H, Teng D, Yang L, Xu X, Chen J, Jiang T, et al. Myeloid-derived itaconate suppresses cytotoxic CD8+ T cells and promotes tumour growth. Nat Metab. 2022; 4: 1660-73.
31. Zhao Y, Liu Z, Liu G, Zhang Y, Liu S, Gan D, et al. Neutrophils resist ferroptosis and promote breast cancer metastasis through aconitate decarboxylase 1. Cell Metab. 2023; 35: 1688-703.
32. Wang X, Su S, Zhu Y, Cheng X, Cheng C, Chen L, et al. Metabolic reprogramming via ACOD1 depletion enhances function of human induced pluripotent stem cell-derived CAR-macrophages in solid tumors. Nat Commun. 2023; 14: 5778.
33. Coffman RL, Sher A, Seder RA. Vaccine adjuvants: putting innate immunity to work. Immunity. 2010; 33: 492-503.
34. Zhang H, Xia X. RNA cancer vaccines: developing mRNA nanovaccine with self-adjuvant property for cancer immunotherapy. Hum Vaccin Immunother. 2021; 17: 2995-8.
35. Zhang H, You X, Wang X, Cui L, Wang Z, Xu F, et al. Delivery of mRNA vaccine with a lipid-like material potentiates antitumor efficacy through Toll-like receptor 4 signaling. Proc Natl Acad Sci U S A. 2021; 118: e2005191118.
36. Ramalho T, Assis PA, Ojelabi O, Tan L, Carvalho B, Gardinassi L, et al. Itaconate impairs immune control of Plasmodium by enhancing mtDNA-mediated PD-L1 expression in monocyte-derived dendritic cells. Cell Metab. 2024; 36: 484-97.
37. Auger J-P, Zimmermann M, Faas M, Stifel U, Chambers D, Krishnacoumar B, et al. Metabolic rewiring promotes anti-inflammatory effects of glucocorticoids. Nature. 2024; 629: 184-92.
38. de Goede KE, Harber KJ, Gorki FS, Verberk SGS, Groh LA, Keuning ED, et al. d-2-Hydroxyglutarate is an anti-inflammatory immunometabolite that accumulates in macrophages after TLR4 activation. Biochim Biophys Acta Mol Basis Dis. 2022; 1868: 166427.
39. Gocher AM, Workman CJ, Vignali DAA. Interferon-γ: teammate or opponent in the tumour microenvironment? Nat Rev Immunol. 2022; 22: 158-72.
40. Chen G, Huang AC, Zhang W, Zhang G, Wu M, Xu W, et al. Exosomal PD-L1 contributes to immunosuppression and is associated with anti-PD-1 response. Nature. 2018; 560: 382-6.
41. Knopf P, Stowbur D, Hoffmann SHL, Hermann N, Maurer A, Bucher V, et al. Acidosis-mediated increase in IFN-γ-induced PD-L1 expression on cancer cells as an immune escape mechanism in solid tumors. Mol Cancer. 2023; 22: 207.
42. Abiko K, Matsumura N, Hamanishi J, Horikawa N, Murakami R, Yamaguchi K, et al. IFN-gamma from lymphocytes induces PD-L1 expression and promotes progression of ovarian cancer. Br J Cancer. 2015; 112: 1501-9.
43. Honce R, Vazquez-Pagan A, Livingston B, Mandarano AH, Wilander BA, Cherry S, et al. Diet switch pre-vaccination improves immune response and metabolic status in formerly obese mice. Nat Microbiol. 2024; 9: 1593-606.
44. Adamik J, Munson PV, Maurer DM, Hartmann FJ, Bendall SC, Argüello RJ, et al. Immuno-metabolic dendritic cell vaccine signatures associate with overall survival in vaccinated melanoma

patients. Nat Commun. 2023; 14: 7211.
45. Shi X, Zhou H, Wei J, Mo W, Li Q, Lv X. The signaling pathways and therapeutic potential of itaconate to alleviate inflammation and oxidative stress in inflammatory diseases. Redox Biol. 2022; 58: 102553.
46. Wu R, Kang R, Tang D. Mitochondrial ACOD1/IRG1 in infection and sterile inflammation. J Intensive Med. 2022; 2: 78-88.
47. McGettrick AF BL, Dorsey FC, O'Neill LAJ. Metabolic Messengers: itaconate. Nat Metab. 2024; 6: 1661-7.
48. Fan Y, Dan W, Wang Y, Ma Z, Jian Y, Liu T, et al. Itaconate transporter SLC13A3 confers immunotherapy resistance via alkylation-mediated stabilization of PD-L1. Cell Metab. 2025; 37: 514-26.
49. Lin H, Tison K, Du Y, Kirchhoff P, Kim C, Wang W, et al. Itaconate transporter SLC13A3 impairs tumor immunity via endowing ferroptosis resistance. Cancer Cell. 2024; 42: 2032-44.
50. Chen C, Liu C, Sun P, Zhang Z, Wang Z, Liu P, et al. Itaconate uptake via SLC13A3 improves hepatic antibacterial innate immunity. Dev Cell. 2024; 59: 2807-17.
51. Wang Z, Cui L, Lin Y, Huo B, Zhang H, Xie C, et al. Cancer cell-intrinsic biosynthesis of itaconate promotes tumor immunogenicity. EMBO J. 2024; 43: 5530-47.
52. Mills EL, Ryan DG, Prag HA, Dikovskaya D, Menon D, Zaslona Z, et al. Itaconate is an anti-inflammatory metabolite that activates Nrf2 via alkylation of KEAP1. Nature. 2018; 556: 113-7.
53. Gu X, Wei H, Suo C, Shen S, Zhu C, Chen L, et al. Itaconate promotes hepatocellular carcinoma progression by epigenetic induction of CD8+ T-cell exhaustion. Nat Commun. 2023; 14: 8154.
54. Chen YJ, Li GN, Li XJ, Wei LX, Fu MJ, Cheng ZL, et al. Targeting IRG1 reverses the immunosuppressive function of tumor-associated macrophages and enhances cancer immunotherapy. Sci Adv. 2023; 9: eadg0654.
55. Weiss JM, Davies LC, Karwan M, Ileva L, Ozaki MK, Cheng RY, et al. Itaconic acid mediates crosstalk between macrophage metabolism and peritoneal tumors. J Clin Invest. 2018; 128: 3794-805.

Figures and Figure legends

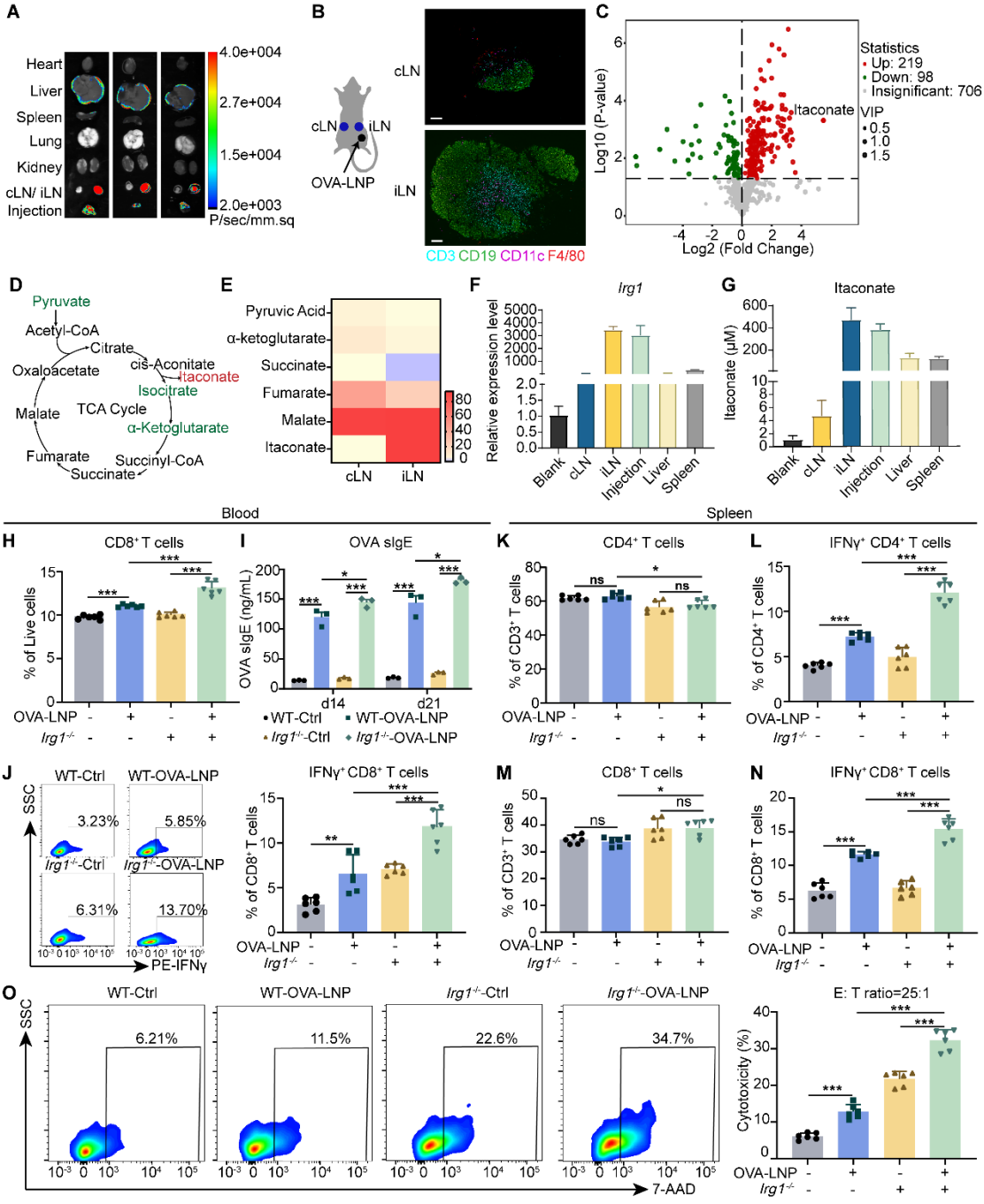

Figure 1

OVA-LNP-induced itaconate suppressed T cell response. (A) The luminescence image of organs in mice after Luciferase-LNP injection for 24h. (B-E) Mice were injected with 5 μg OVA-LNP subcutaneously, and iLNs and cLNs were obtained for metabolome

796 analysis and immunofluorescence at 24 h, n = 5. (B) Immunofluorescence of T cells
797 (CD3), B cells (CD19), DCs (CD11c), and Macrophages (F4/80). scale bars, 100 μm.
798 (C) Volcano plot of different metabolites between iLNs and cLNs. (D) The schematic
799 of the TCA cycle. (E) The heatmap of metabolites of the TCA cycle in iLNs compared
800 to cLNs. (F) *Irg1* mRNA expression of organs in mice after OVA-LNP injection for 24h,
801 n = 3. (G) Itaconate concentration of organs in mice after OVA-LNP injection for 24h,
802 n = 3. (H-O) T-cell and B-cell responses to OVA-LNP in WT and $Irg1^{-/-}$ mice at days
803 14 and 21. (H) The proportion of $CD8^+$ T cells in blood, n = 6. (I) The concentration of
804 OVA sIgE in blood serum was detected by ELISA, n = 3. (J) The percentage of $IFN\gamma^+$
805 $CD8^+$ T cells in blood was detected by flow cytometry, n = 6. (K-N) The proportion of
806 $CD4^+$(K), $IFN\gamma^+$ $CD4^+$(L), $CD8^+$(M), $IFN\gamma^+$ $CD8^+$ (N)T cells in $CD3^+$ T cells isolated
807 from spleens h, n = 6. (O) Cytotoxicity of $CD3^+$ T cells isolated from spleens after being
808 incubated with B16-F10-OVA tumor cells, n = 6. ns = no significance, * $p < 0.05$, ** $p < 0.01$, *** $p < 0.001$.

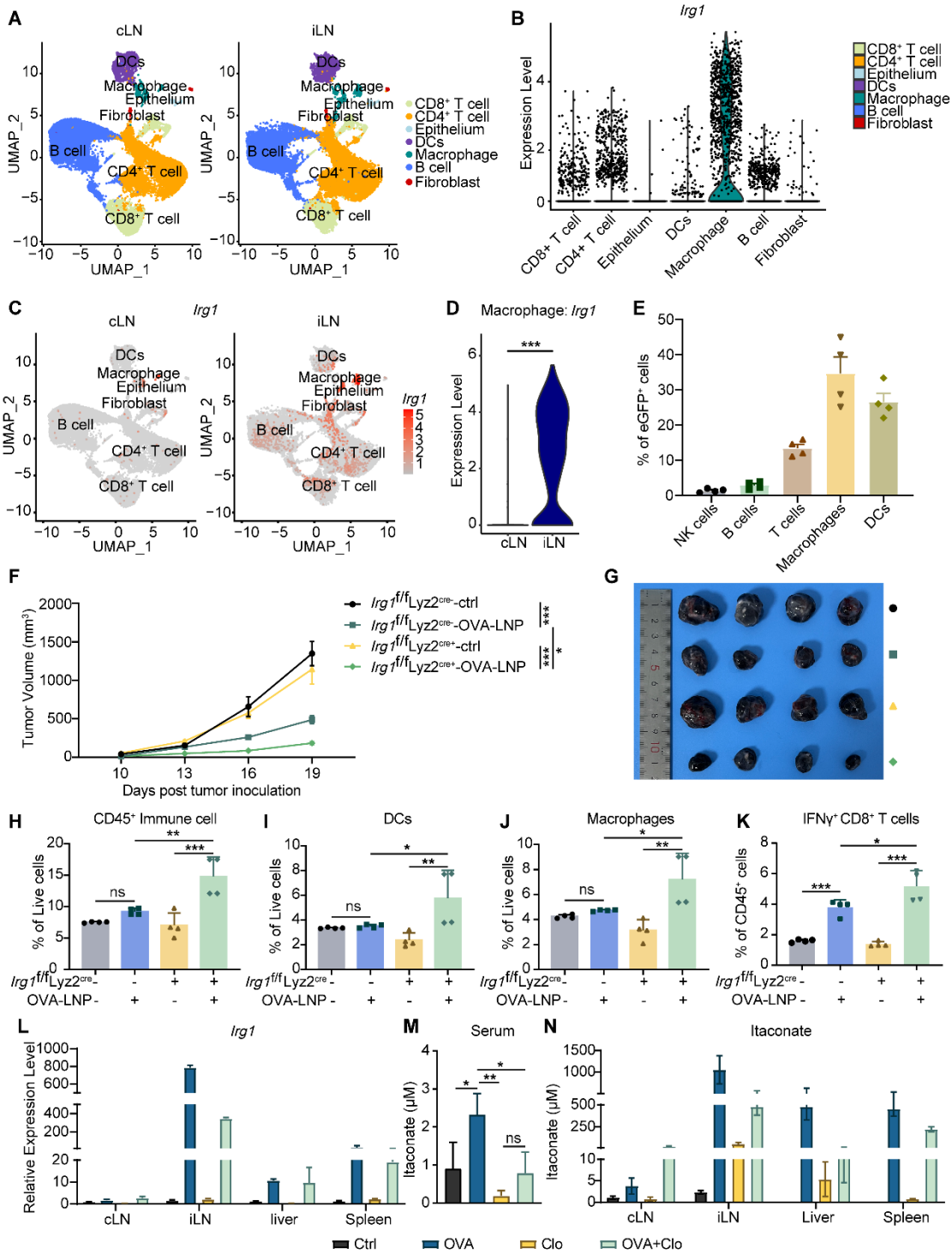

Figure 2

OVA-LNP-induced itaconate derived from macrophages in LNs. (A-D) The single-cell sequence of cLNs and iLNs was collected at 24 h after the OVA-LNP injection, n = 5. (A) The UMAP visually represented different immune cell types in cLN and iLN. (B)

Irg1 expression levels of different immune cells in LNs. (C) The UMAP plot depicted the expression levels of *Irg1* in cLNs and iLNs. (D) Comparing the *Irg1* expression levels of macrophages in cLNs and iLNs. (E) The different types of immune cells in iLNs, such as NK cells (NK1.1), B cells (CD19), T cells (CD3), Macrophages (F4/80), and DCs (CD11c), were detected using flow cytometry at 24 h after subcutaneous injection of eGFP-LNP. (F-K) The therapeutic effect and the TME remodeling of OVA-LNP in $Irg1^{f/f}$ Lyz2 $^{cre-}$ (n = 4) and $Irg1^{f/f}$ Lyz2 $^{cre+}$ (n = 4) mice. (F) Tumor growth curve of ctrl and two-dose 5 μg OVA-LNP treatment on days 7 and 12 in $Irg1^{f/f}$ Lyz2 $^{cre-}$ and $Irg1^{f/f}$ Lyz2 $^{cre+}$ mice. (G) Tumor image on day 21. (H to K) The percentage of $CD45^+$ immune cells (H), DCs (I), macrophages (J), and $IFN\gamma^+$ $CD8^+$ T cells (K) within the TME between four groups. (L) *Irg1* mRNA expression of organs in mice with Clo at day 1 and OVA-LNP at day 2 for 24h, n = 3. (M-N) The concentration of itaconate in the blood (M) and organs (N) in mice with Clo at day 1 and OVA-LNP at day 2 for 24h, n = 3. ns = no significance, * $p < 0.05$, ** $p < 0.01$, *** $p < 0.001$.

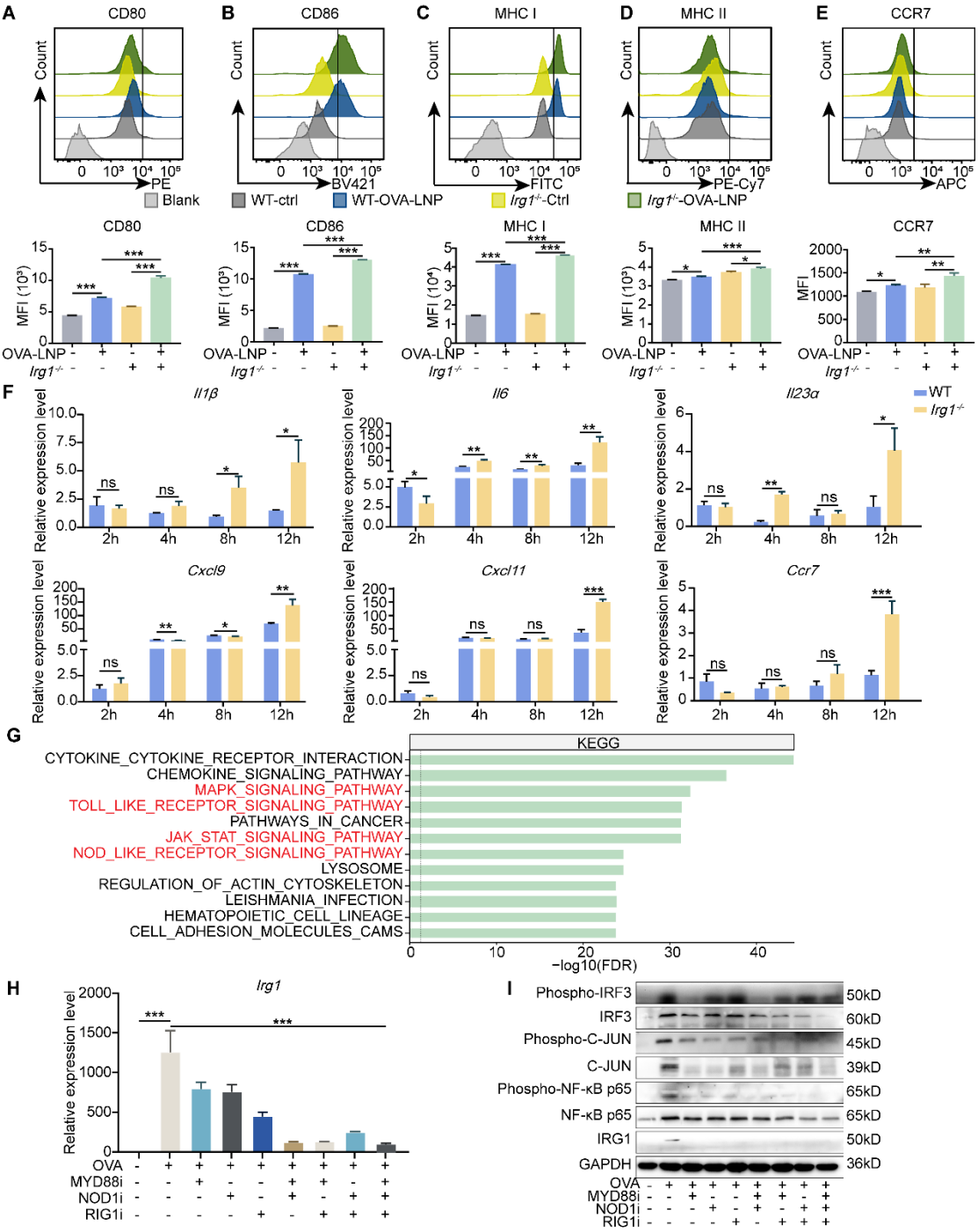

Figure 3

Irg1-induced by OVA-LNP suppressed the pro-inflammatory of macrophages. (A-E) The activation makers of WT and *Irg1*$^{-/-}$ macrophages were detected by flow cytometry at 24 h after being stimulated by 0.3 μg/mL ctrl-LNP or OVA-LNP. CD80 (A), CD86 (B), MHC I (C), MHC II (D), and CCR7 (E) levels of macrophages, n = 3. (F) The *Il1β,*

Il6, Il23α, Cxcl9, Cxcl10, and *Ccr7* expression levels of WT and *Irg1*$^{-/-}$ macrophages, which were stimulated by 0.3 μg/mL ctrl-LNP or OVA-LNP at 2, 4, 8, 12 h, were measured by qRT-PCR, n = 3. (G) Kyoto Encyclopedia of Genes and Genomes (KEGG) enrichment of macrophages in iLNs compared to cLNs. (H) qRT-PCR measured expression levels of *Irg1* in BMDMs after treatment with 0.3 μg/mL OVA-LNP and 10 μM MYD88 inhibitor (MYD88i), 10 μM NOD1 inhibitor (NOD1i), and 500 nM RIG1 inhibitor (RIG1i) for 12 h, n = 3. (I) BMDMs were treated with 0.3 μg/mL OVA-LNP and 10 μM MYD88 inhibitor (MYD88i), 10 μM NOD1 inhibitor (NOD1i), and 500 nM RIG1 inhibitor (RIG1i) for 24 h, and cells were collected for western blot analysis. ns = no significance, * $p < 0.05$, ** $p < 0.01$, *** $p < 0.001$.

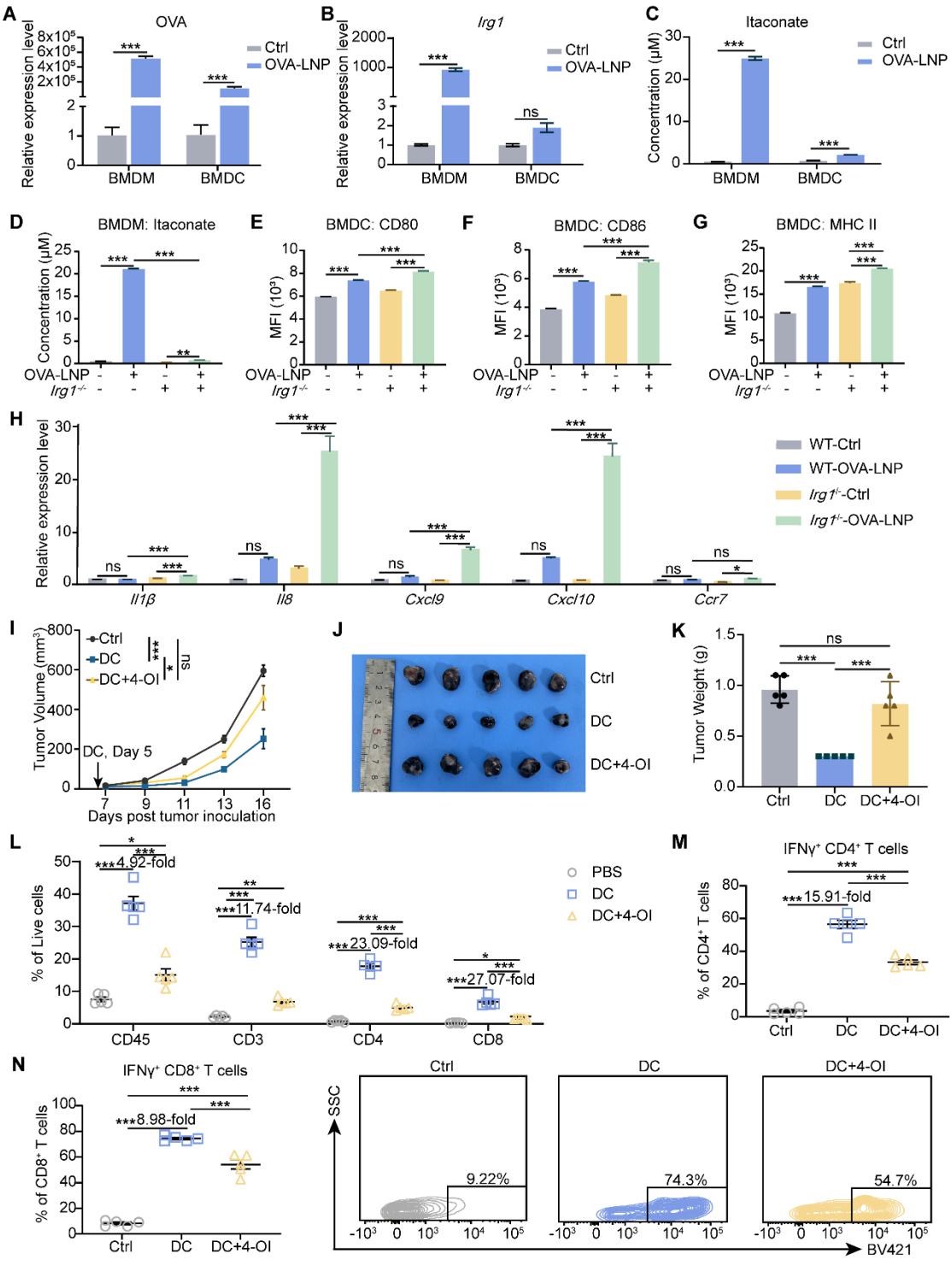

Figure 4

OVA-LNP-induced itaconate suppressed the function of DCs. (A-B) OVA (A) and *Irg1* (B) expression of BMDMs and BMDCs with 0.3 μg/mL OVA-LNP stimulation for 12 h, n = 3. (C) LC/MS measured the concentration of itaconate in the supernatant of

BMDM and BMDC after 24 h of OVA-LNP stimulation, n = 3. (D) The concentration of itaconate in the WT and *Irg1*$^{-/-}$ BMDM supernatant. (E-G) CD80 (E), CD86 (F), and MHC II (G) of BMDCs cultured with BMDMs CM for 24 h were measured by flow cytometry, n = 3. (H) The *Il1β, Il8, Cxcl9, Cxcl10*, and *Ccr7* expression levels of BMDC cultured with BMDM CM for 12 h were measured by qRT-PCR, n = 3. (I-K) The anti-tumor activity and TME remodeling by 4-OI-treated DCs in C57BL/6 mice, n = 5. The tumor growth curve (I), tumor image (J), and tumor weight (K) of B16-F10-OVA-beared mice after administration with DCs or 4-OI-treated DCs subcutaneously at day 5. (L) The proportion of immune cells and $CD3^+$, $CD4^+$, and $CD8^+$ T cells within TME after treatment with DCs or 4-OI-treated DCs compared to the control group. (M) The percentage of $IFN\gamma^+$ $CD4^+$ T cells among $CD4^+$T cells in the TME. (N) The statistics and presentative data of $IFN\gamma^+$ $CD8^+$ T cells in the TME. ns = no significance, * $p < 0.05$, ** $p < 0.01$, *** $p < 0.001$.

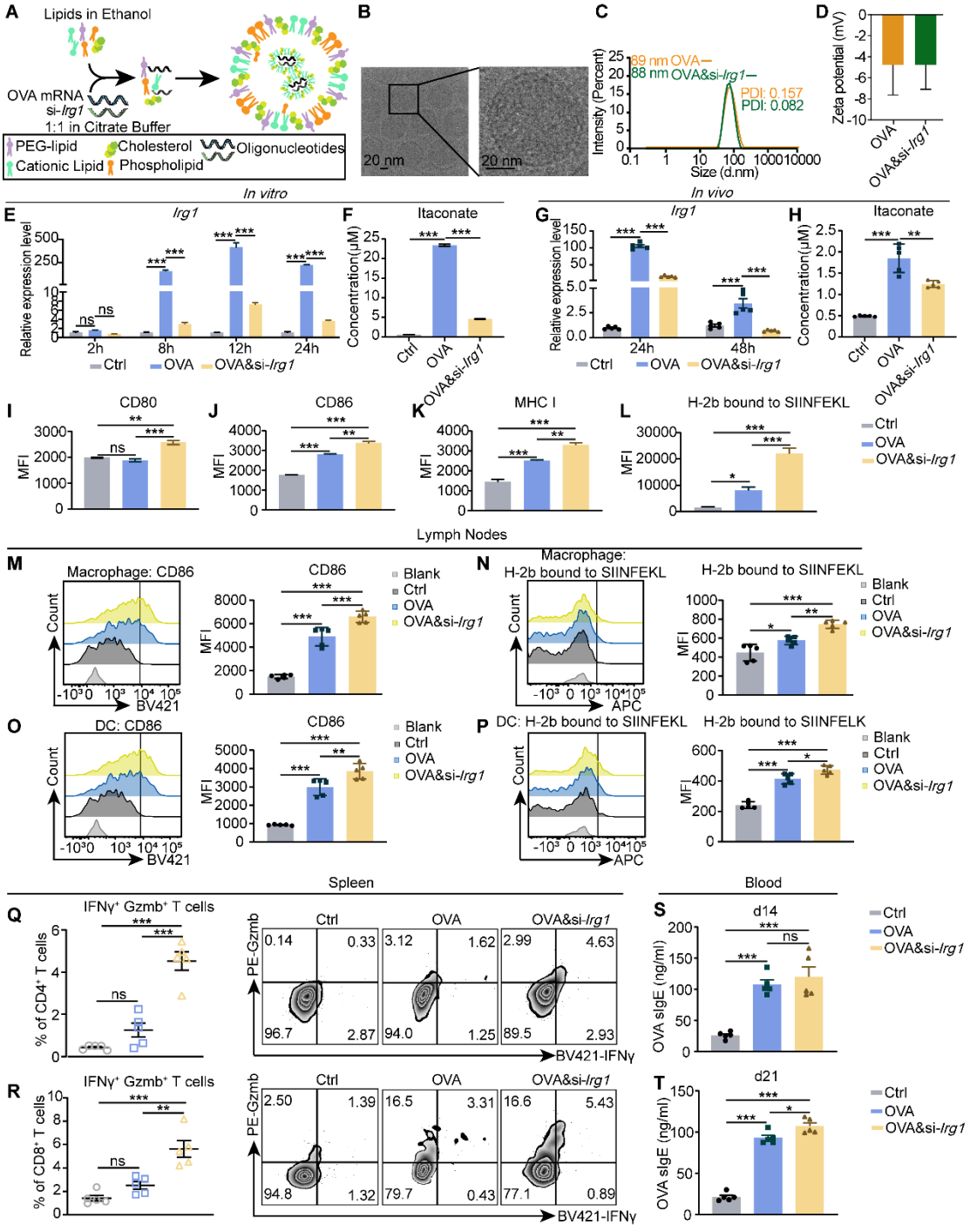

Figure 5

Targeting *Irg1* on macrophages in LNs. (A) The diagram of the process of encapsulating OVA&si-*Irg1*-LNP. (B) The structure of OVA&si-*Irg1*-LNP by cryo-TEM. (C-D) The diameter (C) and zeta potential (D) of OVA-LNP and OVA&si-*Irg1*-LNP. (E) *Irg1* expression levels of BMDM after treatment with 0.3 μg/mL OVA-LNP and OVA&si-

Irg1-LNP for different time points detected by qRT-PCR, n = 3. (F) The itaconate concentration of supernatant of BMDM after treatment with 0.3 μg/mL OVA-LNP and OVA&si-*Irg1*-LNP for 24 h was detected by LC/MS, n = 3. (G) *Irg1* expression levels of LNs after treatment with 5 μg OVA-LNP and OVA&si-*Irg1*-LNP subcutaneously for 24 and 48 h were detected by qRT-PCR, n = 5. (H) The itaconate concentration of intertissue fluid of LNs after treatment with 5 μg OVA-LNP and OVA&si-*Irg1*-LNP for 24 h was detected by LC/MS. (I-L) CD80 (I), CD86 (J), MHC I (K), and H-2^b bound to SIINFEKL (L) of BMDM after treatment with 0.3 μg/mL OVA-LNP and OVA&si-*Irg1*-LNP for 24 h were detected by flow cytometry, n = 3. (M-P) The CD86 and H-2^b bound to SIINFEKL of macrophages (M and N) and DC (O-P) in LNs after treatment with 5 μg OVA-LNP and OVA&si-*Irg1*-LNP subcutaneously in C57BL/6 mice for 24 h were detected by flow cytometry, n = 5. (Q-R) The statistic and presentative data of IFNγ$^+$ Gzmb$^+$ CD4$^+$(Q), IFNγ$^+$ Gzmb$^+$ CD8$^+$ (R) T cells in spleens were detected by flow cytometry after treatment with 5 μg OVA-LNP and OVA&si-*Irg1*-LNP subcutaneously in C57BL/6 mice for 21 days, n = 5. (S-T) The concentration of OVA sIgE in blood serum at days 14 (S) and 21 (T) was detected by ELISA with 5 μg OVA-LNP and OVA&si-*Irg1*-LNP injection subcutaneously, n = 5. ns = no significance, * $p < 0.05$, ** $p < 0.01$, *** $p < 0.001$.

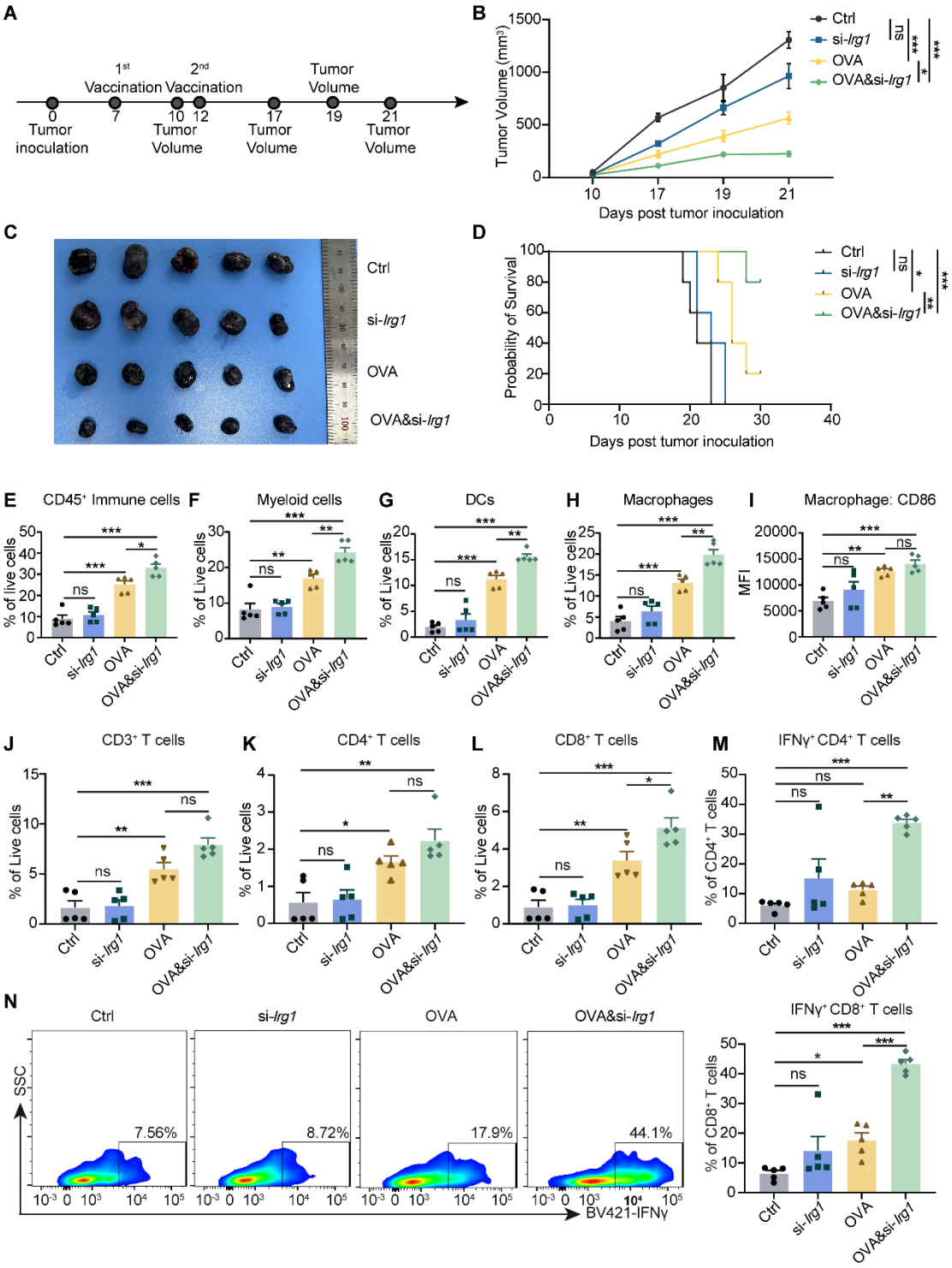

Figure 6

OVA&si-*Irg1*-LNP promoted therapeutic efficacy and remodeled the tumor microenvironment in the B16-F10 melanoma mouse model. (A)The schematic diagram of the B16-F10-OVA-beared melanoma mouse model, n = 5. (B-C) The tumor growth

curve (B) and tumor image (C) of the B16-F10-beared mice after administration with two-dose LNPs. (D) Kaplan-Meier analysis of B16-F10-OVA melanoma mice. (E-N) The percentage of immune cells in the TME was detected by flow cytometry after LNP treatment for 21 days. (E-I) The proportion of $CD45^+$ immune cells (E), $CD11b^+$ myeloid cells (F), $CD11c^+$ DCs (G), $F4/80^+$ macrophages (H), CD86 expression level of macrophages (I) within TME. (J-N) Flow cytometry analysis of $CD3^+$ (J), $CD4^+$ (K), $CD8^+$ (L), $IFN\gamma^+$ $CD4^+$ (M) T cells, and the presentative and statistic proportion of $IFN\gamma^+$ $CD8^+$ T cells (N) in the TME after LNPs treatment. ns = no significance, * $p < 0.05$, ** $p < 0.01$, *** $p < 0.001$.

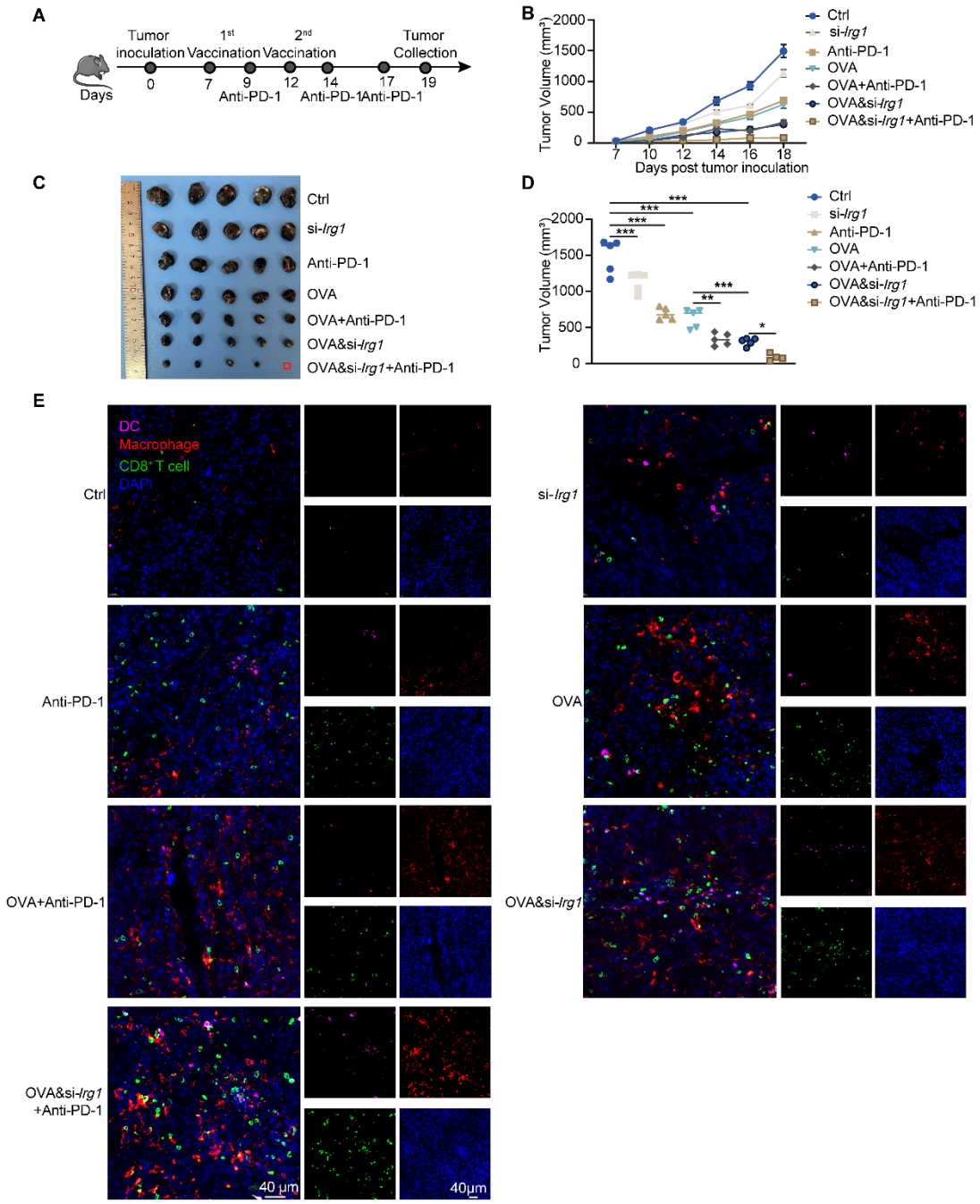

Figure 7

OVA&si-*Irg1*-LNP enhanced the anti-tumor efficacy of anti-PD-1 antibody. (A) The schematic diagram showed the administration of LNPs alone or combined with an anti-PD-1 antibody in a B16-F10-OVA-bearing melanoma mouse model, n = 5. (B-D) The tumor growth (B), tumor image (C), and tumor volume at day 19 (D) of the B16-F10-OVA-beared mice. (E) The immune cells, like DCs (CD11b), macrophage (F4/80), and

908 $CD8^+$ T cells (CD8), were detected by immunofluorescence in the TME. ns = no

909 significance, * $p < 0.05$, ** $p < 0.01$, *** $p < 0.001$.